The Astrophysical Journal Letters, 754:L34 (6pp), 2012 August 1 doi:10.1088/2041-8205/754/2/L34

THE INFRARED EYE OF THE WIDE-FIELD CAMERA 3 ON THE *HUBBLE SPACE TELESCOPE* REVEALS MULTIPLE MAIN SEQUENCES OF VERY LOW MASS STARS IN NGC 2808*

A. P. Milone[1,2], A. F. Marino[3], S. Cassisi[4], G. Piotto[5,6], L. R. Bedin[6], J. Anderson[7], F. Allard[8], A. Aparicio[1,2], A. Bellini[7], R. Buonanno[4,9], M. Monelli[1,2], and A. Pietrinferni[4]

[1] Instituto de Astrofìsica de Canarias, E-38200 La Laguna, Tenerife, Canary Islands, Spain; milone@iac.es, aparicio@iac.es, monelli@iac.es
[2] Department of Astrophysics, University of La Laguna, E-38200 La Laguna, Tenerife, Canary Islands, Spain
[3] Max-Planck-Institut für Astrophysik, Karl-Schwarzschild-Str. 1, D-85741 Garching Bei München, Germany; amarino@MPA-Garching.MPG.DE
[4] INAF-Osservatorio Astronomico di Collurania, Via Mentore Maggini, I-64100 Teramo, Italy; cassisi@oa-teramo.inaf.it, pietrinferni@oa-teramo.inaf.it
[5] Dipartimento di Astronomia, Università di Padova, Vicolo dell'Osservatorio 3, Padova I-35122, Italy; giampaolo.piotto@unipd.it
[6] INAF-Osservatorio Astronomico di Padova, Vicolo dell'Osservatorio 5, I-35122 Padova, Italy; luigi.bedin@oapd.inaf.it
[7] Space Telescope Science Institute, 3800 San Martin Drive, Baltimore, MD 21218, USA; jayander@stsci.edu, bellini@stsci.edu
[8] CRAL, UMR 5574, CNRS, Universitè de Lyon, Ècole Normale Supèrieure de Lyon, 46 Allèe d'Italie, F-69364 Lyon Cedex 07, France; france.allard@me.com
[9] Dipartimento di Fisica, Universitá di Roma Tor Vergata, Via della Ricerca Scientifica 1, I-00133 Rome, Italy; buonanno@roma2.infn.it
Received 2012 May 21; accepted 2012 June 19; published 2012 July 17

ABSTRACT

We use images taken with the infrared channel of the Wide Field Camera 3 on the *Hubble Space Telescope* to study the multiple main sequences (MSs) of NGC 2808. Below the turnoff, the red, the middle, and the blue MS, previously detected from visual-band photometry, are visible over an interval of about 3.5 F160W magnitudes. The three MSs merge together at the level of the MS bend. At fainter magnitudes, the MS again splits into two components containing ∼65% and ∼35% of stars, with the most-populated MS being the bluest one. Theoretical isochrones suggest that the latter is connected to the red MS discovered in the optical color–magnitude diagram (CMD) and hence corresponds to the first stellar generation, having primordial helium and enhanced carbon and oxygen abundances. The less-populated MS in the faint part of the near-IR CMD is helium-rich and poor in carbon and oxygen, and it can be associated with the middle and the blue MS of the optical CMD. The finding that the photometric signature of abundance anti-correlation is also present in fully convective MS stars reinforces the inference that they have a primordial origin.

Key words: globular clusters: individual (NGC 2808) – Hertzsprung–Russell and C–M diagrams

Online-only material: color figures

1. INTRODUCTION

In recent years, photometric studies have shown that the color–magnitude diagrams (CMDs) of globular clusters (GCs) can be very complex, with the presence of multiple main sequences (MSs, e.g., Anderson 1997; Bedin et al. 2004; Piotto et al. 2007, hereafter P07), multiple subgiant branches (e.g., Milone et al. 2008, 2012a, Anderson et al. 2009; Piotto et al. 2012), and multiple or spread red-giant branches (RGBs, e.g., Yong et al. 2008; Marino et al. 2008; Lee et al. 2009).

Photometric and spectroscopic investigations have revealed that the multiple sequences in the CMDs of many GCs are populated by stars with different helium and light-element abundances (e.g., Piotto et al. 2005, 2007; Yong et al. 2008; Marino et al. 2008; Sbordone et al. 2011, hereafter S11). In some cases, the presence of stellar populations with different compositions (in particular, helium) has been associated with the presence of multimodal or extended horizontal branches (HBs; e.g., D'Antona et al. 2005, P07; D'Antona & Caloi 2008; Marino et al. 2011).

Among clusters with multiple stellar populations, NGC 2808 is certainly one of the most intriguing objects. Its CMD shows a multimodal MS (D'Antona et al. 2005) composed of three distinct components (P07; Milone et al. 2012a, hereafter M12), a multimodal HB, which is greatly extended blueward (Sosin et al. 1997; Bedin et al. 2000), and a spread RGB (Lee et al. 2009). Furthermore, spectroscopic studies of RGB, HB, and bright MS stars have revealed significant star-to-star variations in the light-element abundances, with three distinct groups of stars populating an extended Na–O anti-correlation (Carretta et al. 2006; Gratton et al. 2011; Bragaglia et al. 2010).

Photometric studies based on data collected with the Wide Field Channel of the Advanced Camera for Surveys (WFC/ACS) on board the *Hubble Space Telescope* (*HST*) have made it possible to detect and characterize the multiple MSs of NGC 2808 from the MSTO down to about 4 mag below the MSTO (P07; M12): the stars all have almost the same age and [Fe/H] but different helium and light-element abundances. The red MS (rMS) corresponds to a first generation and has primordial helium and light-element abundances ($Y \sim 0.25$), while the blue (bMS) and the middle (mMS) include later generations of stars, and are both enhanced in helium, sodium, and nitrogen ($Y \sim 0.38$ and $Y \sim 0.32$, respectively) and depleted in oxygen and carbon (D'Antona et al. 2005; P07).

Usually, photometry of GC sequences extends over a limited spectral region, from the ultraviolet ($\lambda \sim 2000$ Å) to the near-infrared (NIR, $\lambda \sim 8000$ Å). As such, multiple sequences are rarely detected along the lower part of the MS, because observational limits make it hard to get high-accuracy photometry of very faint and red stars in optical and UV colors.

In this Letter, we use *HST* to extend the study to the near-infrared passbands and complement the work by S11 who analyzed the signatures of the anti-correlations in the visual and ultraviolet portion of the spectrum. We analyze the CMD

* Based on observations with the NASA/ESA *Hubble Space Telescope*, obtained at the Space Telescope Science Institute, which is operated by AURA, Inc., under NASA contract NAS 5-26555.

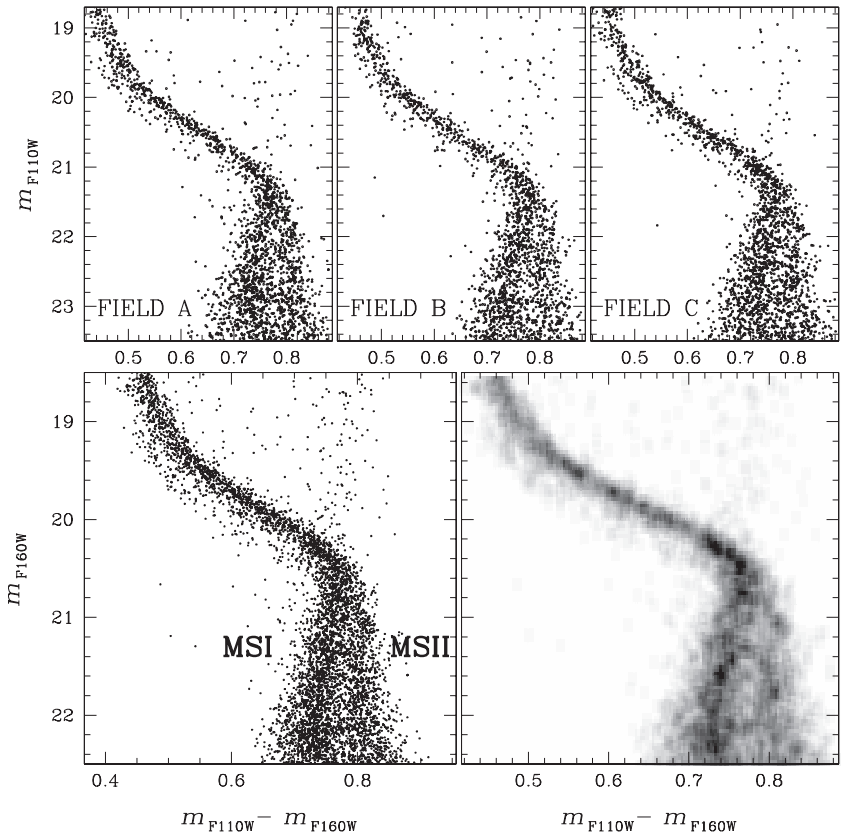

Figure 1. Upper panels: m_{F110W} vs. $m_{F110W} - m_{F160W}$ CMD for stars in the fields "A", "B," and "C" corrected for differential reddening. Lower panels: m_{F160W} vs. $m_{F110W} - m_{F160W}$ CMD (left) and Hess diagram (right) for all the stars.

of NGC 2808 through the F110W ($\sim J$) and F160W ($\sim H$) filters of the infrared channel of the Wide Field Camera 3 (WFC3/IR) and follow, for the first time, the multiple sequences of this cluster over a wide interval of stellar masses, from the turnoff down to very low mass (VLM) MS stars ($\mathcal{M} \sim 0.2\ \mathcal{M}_{\odot}$).

2. OBSERVATIONS AND DATA REDUCTION

In this work, we used archival *HST* images taken with the WFC3/IR camera for program GO-11665 (PI: Brown). This data set consists of 2 × 699 s exposures through F110W and two through F160W of 799 s and 899 s for each of three different WFC3/NIR fields, taken in parallel while STIS was taking spectra of EHB stars. All fields are located at about 6 arcmin from the cluster center.

In the following, fields "A", "B," and "C" will correspond, respectively, to the fields in the southwest, south, and northeast of the cluster center. Field "A" partially overlaps the ACS/WFC field analyzed by P07 and M12. Therefore, for a subsample of the measured stars, we have both visual and NIR photometry and can perform a direct comparison of the multi-band photometry (see Section 3).

The images were reduced by using a software package that is based largely on the algorithms described by Anderson & King (2006) and will be presented in a separate paper. Star positions are corrected for geometric distortion by using the solution given by A. J. Anderson et al. (2012, in preparation) and were calibrated as in Bedin et al. (2005) using the current online estimates for zero points and encircled energies.[10]

[10] http://www.stsci.edu/hst/wfpc3/phot_zp_lbn

The analysis we present here requires high-precision photometry, so we selected a high-quality sample of stars that (1) have a good fit to the point-spread function, (2) are relatively isolated, (3) and have small astrometric and photometric errors (see Milone et al. 2009, Section 2.1 for details of this procedure). Finally we corrected our photometry for differential reddening using the method that is described in great detail in Milone et al. (2012b). Briefly, the method consists of defining an MS ridge line in the CMD. Then, for each star, we selected the 35 nearest well-measured neighbors and evaluated for each of them the color distance from the fiducial line along the reddening line. We applied to the target star a correction equal to the median color distance of these 35 stars.

3. THE NIR COLOR–MAGNITUDE DIAGRAM OF NGC 2808

The IR m_{F110W} versus $m_{F110W} - m_{F160W}$ CMDs of stars in the fields "A", "B," and "C" are plotted in the upper panels of Figure 1, while the lower left and lower right panels show the m_{F160W} versus $m_{F110W} - m_{F160W}$ CMD and the Hess diagram for all the stars. The most obvious feature in these diagrams is the multi-modal MS that stretches from the turnoff (just below saturation) to about three F160W magnitudes below it. Furthermore, the MS's breadth and color distribution dramatically change when moving from bright to faint magnitudes. Down to $m_{F160W} \sim 20.5$, the color distribution across the MSs is consistent with what has been previously observed in the optical. As expected from theory, below this, the MS runs almost vertically (actually slightly shifting toward bluer colors), and the three MS components discovered by P07 appear to merge at

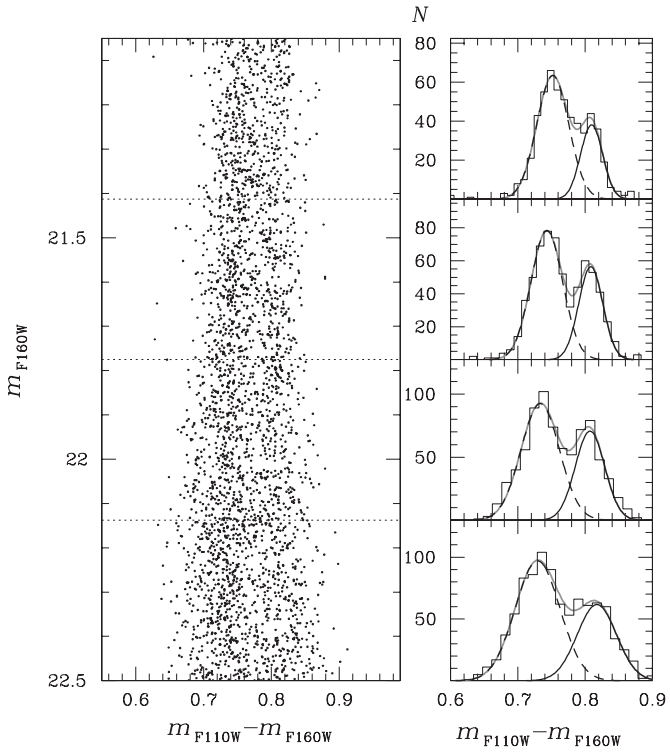

Figure 2. Left panel: a close-up of the region of the m_{F160W} vs. $m_{F110W}-m_{F160W}$ CMD from the lower left panel of Figure 1, where the MS split is more evident. Right panel: the color distribution of the stars plotted in the left panel, in four F160W magnitude intervals. The continuous gray lines are fits by a sum of two Gaussians.

this bending point. However, below $m_{F160W} \sim 21$, the MS split re-appears, but this time with a different morphology. Whereas in the upper part of the CMD, and as in the optical bands, the less-populated MS is the bluest component, below $m_{F160W} \sim 21$, the less-populated component is the reddest one. In the following, we will refer to these two MS components fainter than $m_{F160W} \sim 21$, as MS_I (more-populated MS and bluer) and MS_{II} (less-populated MS and redder).

To estimate the fraction of stars in each MS we followed the procedure illustrated in Figure 2, which is similar to that used in several previous papers (e.g., P07). The left panel shows a zoom-in of the m_{F160W} versus $m_{F110W} - m_{F160W}$ CMD region where the MS split is most evident. We analyze the color distribution of the stars plotted in the left panel in four magnitude intervals over the range $21.25 < m_{F160W} < 22.5$. The distribution is clearly bimodal and has been fitted with two Gaussians (dashed and continuous black lines for the MS_I and MS_{II}, respectively). From the areas under the Gaussians, we find that $65\% \pm 2\%$ of stars belong to the MS_I, and $35\% \pm 2\%$ to the MS_{II}. The errors are calculated as the rms of the measurements obtained in the $N = 4$ mag intervals divided by $\sqrt{N-1}$.

We note that the fractions of stars along MS_I and MS_{II} are very similar to the fraction of rMS ($62\% \pm 2\%$) stars and the total fraction of mMS and bMS stars ($24 + 14 = 38\% \pm 3\%$; M12). This fact makes it very tempting to associate the MS_I with the rMS (defined by P07), while both their mMS and their bMS could be the extension to bright magnitudes of the MS_{II}. To further investigate this issue, in Figure 3, we show photometry for the stars in field "A" that also happen to be measured in P07. The three groups—bMS, mMS, and rMS—defined in P07 are colored in blue, green, and red, and are plotted with the same color code in the other panels. In the upper right panel, we show the m_{F160W} versus $m_{F110W} - m_{F160W}$ CMD for the same stars cross-identified in the WFC3/NIR bandpasses. We note that (1) *above* the MS bend ($m_{F160W} \simeq 20.5$) the three MSs exhibit the same relative locations in the NIR as in the optical CMD, (2) *at* the magnitude of the MS bend, the three MSs appear to merge, and (3) *below* the MS bend, the bMS and mMS appear to become redder than the stars labeled as rMS in the optical photometry. The histograms of the NIR color distribution in the inset of the top right panel of Figure 3 appear to confirm this trend. The cyan and the red histograms show the color distribution for bMS+mMS stars and rMS, respectively, in the magnitude interval $20.75 < m_{F160W} < 21.00$. The cyan histogram (bMS+mMS) has, on average, bluer colors than the red histogram (rMS).

In the lower left panel, we show the NIR fiducial lines for the optically selected rMS sample of stars (in red). Defining this fiducial line is an iterative procedure. We started from our optically defined sample of rMS stars (from P07 and M12), then we calculated the sigma-clipped median of NIR colors and of NIR magnitudes for rMS stars in intervals of 0.2 mag in F160W, and interpolated with a spline. Similarly, we obtained the fiducial lines for the combined sample of mMS and bMS stars shown in the middle panel. The two fiducial lines are compared in the lower right panel and confirm that the rMS is indeed redder than the mMS and bMS for magnitudes fainter than $m_{F160W} \sim 20.6$. It is therefore legitimate to associate the rMS with the component MS_I, and bMS+mMS with the MS_{II}.

4. DISCUSSION

The near-IR/WFC3 CMD presented in this Letter allows us to examine, for the first time, the behavior of multiple MSs among VLM stars. As expected, in the near-IR, the MS stars less massive than $\sim 0.4\,M_\odot$ define a sequence with nearly constant color (see, e.g., Baraffe et al. 1997; Zoccali et al. 2000; Calamida et al. 2009; Bono et al. 2010, and references therein). Theoretical models predict that this is due to two competing effects. On one hand, the increase of the radiative opacity, coupled with the decrease of the effective temperature, shifts the stellar colors to the red. On the other hand, the increase of the collisional-induced absorption (CIA) of the H_2 molecule in the infrared moves the stellar flux back to the blue. In a given range of stellar masses, the two effects compensate for each other, and the MS locus runs almost vertical. Moving toward less massive stars, the second effect becomes dominant, and the color of the MS becomes bluer and bluer with decreasing stellar mass. The CIA source is obviously related to the abundance of H_2 molecules. It also scales as the square of the density (ρ), as opposed to other opacity sources, which are proportional to ρ (Cassisi 2012, and references therein).

In order to compare empirical evidence with suitable evolutionary predictions, we have computed some grids of evolutionary models for both low and very low mass stars. For the low-mass structures (i.e., $\mathcal{M} > 0.5\,\mathcal{M}_\odot$) we adopt the physical scenario described in Pietrinferni et al. (2006), while in the VLM regime we use the same physical inputs adopted in Cassisi et al. (2000). We address the interested reader to the quoted references for details. The match between the more massive models and the VLM models was made at a mass level where the transition in luminosity and effective temperature between the two regimes is smooth (usually $\sim 0.5\,\mathcal{M}_\odot$). We computed stellar models for an iron content equal to $[Fe/H] = -1.3$, and α-element enhancement equal to $[\alpha/Fe] = +0.4$, and for three values for the initial He abundances: $Y = 0.248$, 0.35, and

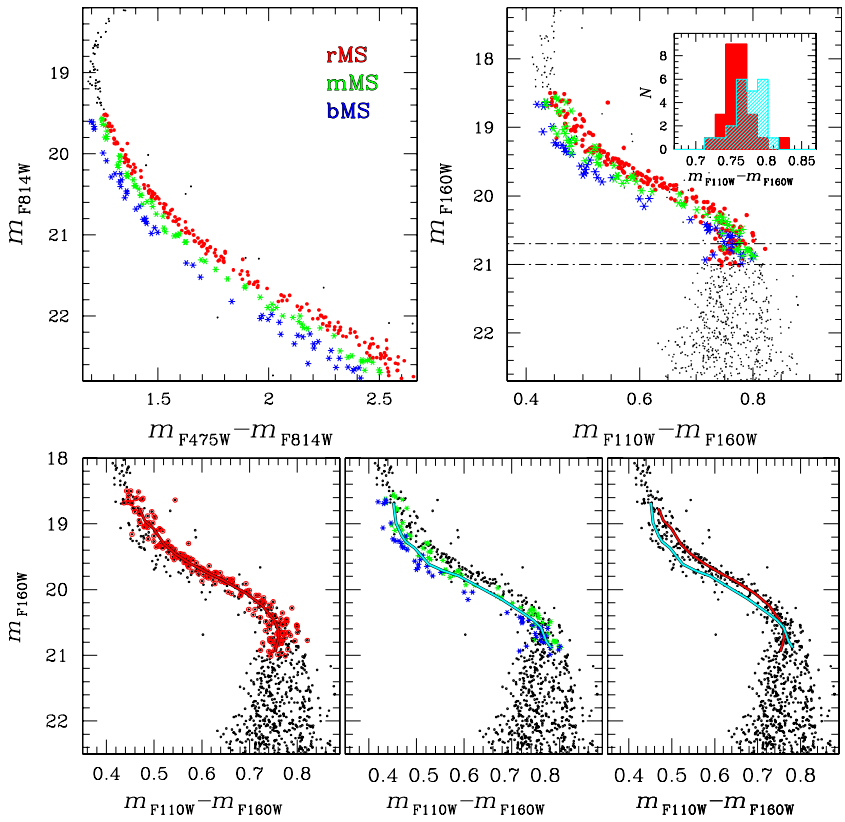

Figure 3. Upper panels: m_{F814W} vs. $m_{F475W} - m_{F814W}$ (left) and m_{F160W} vs. $m_{F110W} - m_{F160W}$ CMD for stars in field "A" (right). The rMS, mMS, and bMS stars are colored red, green, and blue, respectively. The color distribution for MS stars between the two dashed-dotted lines is shown in the inset where red and cyan histograms correspond to rMS stars and to the sample of both mMS and bMS stars, respectively (see the text for details). Lower panels: fiducial line for the rMS stars (left) and for stars in the other two MSs (middle) superimposed on the IR CMD. A comparison of the two fiducial lines is shown in the right panel.

(A color version of this figure is available in the online journal.)

0.40, namely. These initial He abundances have been selected on the basis of the comparison between stellar models and the triple MS observed in the optical CMD of NGC 2808 performed by P07.

The theoretical models have been transformed into the observational domain by integrating the synthetic spectra of the BT-Settl AGSS model atmosphere grid[11] (Allard et al. 2011, 2012) over the IR WFC3 bandpasses. We used the filter transmission tables provided by the System Throughputs Web site for the WFC3.

The upper left panel of Figure 4 shows the location in the selected near-IR CMD of 12 Gyr isochrones for the selected assumptions about the initial He abundances. Data in Figure 4 show that for $m_{F160W} \lesssim 21$, i.e., $M_{F160W} \lesssim 6$, the He abundance plays a fundamental role in driving the MS location: when increasing the He abundance from $Y = 0.248$ to 0.40 the MS locus becomes fainter by more than 0.5 mag at fixed color. This is consistent (and indeed explains) the separation of the three MSs observed in the upper part ($m_{F160W} < 20.5$) of the CMDs of Figures 1 and 3. However, since helium-rich stars have lower hydrogen abundance, we would expect that, in the stellar mass regime where the two (previously quoted) physical processes are in competition, the He-rich VLM stars would appear redder than He-normal stars for their lower H_2 abundance, and consequent lower contribution coming from the H_2 CIA. Indeed, at fainter magnitudes, the He-normal ($Y = 0.248$) MS sequence runs on the blue side of the more He-rich sequences, but the effect is very small, smaller than the observed one.

We note that, below the faint limit of our photometry ($M_{F160W} \lesssim 10$), the He-normal sequence reaches fainter magnitudes and bluer colors than the He-rich counterpart. This is an important feature that could be tested with deeper CMDs and may represent an independent observational confirmation of high-He enhancement.

The bottom left panel of Figure 4 shows that the difference in the initial He abundances among the stars belonging to the distinct MS loci is not able to provide a complete explanation of the observed trend. In the following, we will attempt to identify the origin of the (small) separation of the observed MSs at magnitudes fainter than $M_{F160W} \sim 20.5$. First of all, we note that the model atmospheres adopted for computing the color–T_{eff} transformations do not account for the peculiar chemical patterns of the various subpopulations present in NGC 2808. In particular, they do not take into account the effect of light elements anti-correlations, which have been shown to be relevant for the MS color in the UV and Strömgren bands (S11; M12).

In order to explore the impact of light-element variations on the NIR WFC3 bands, we have computed synthetic spectra trying to account for the chemical patterns of the stars belonging to the distinct MSs in NGC 2808. For this calculation, we used the ATLAS9 and SYNTHE Kurucz programs in the range from 8000 Å to 18000 Å (Kurucz 2005; Sbordone et al. 2007).[12]

[11] These model atmospheres and color tables are available via the Phoenix Web simulator at the following URL: http://phoenix.ens-lyon.fr/simulator.

[12] http://wwwuser.oat.ts.astro.it/castelli/

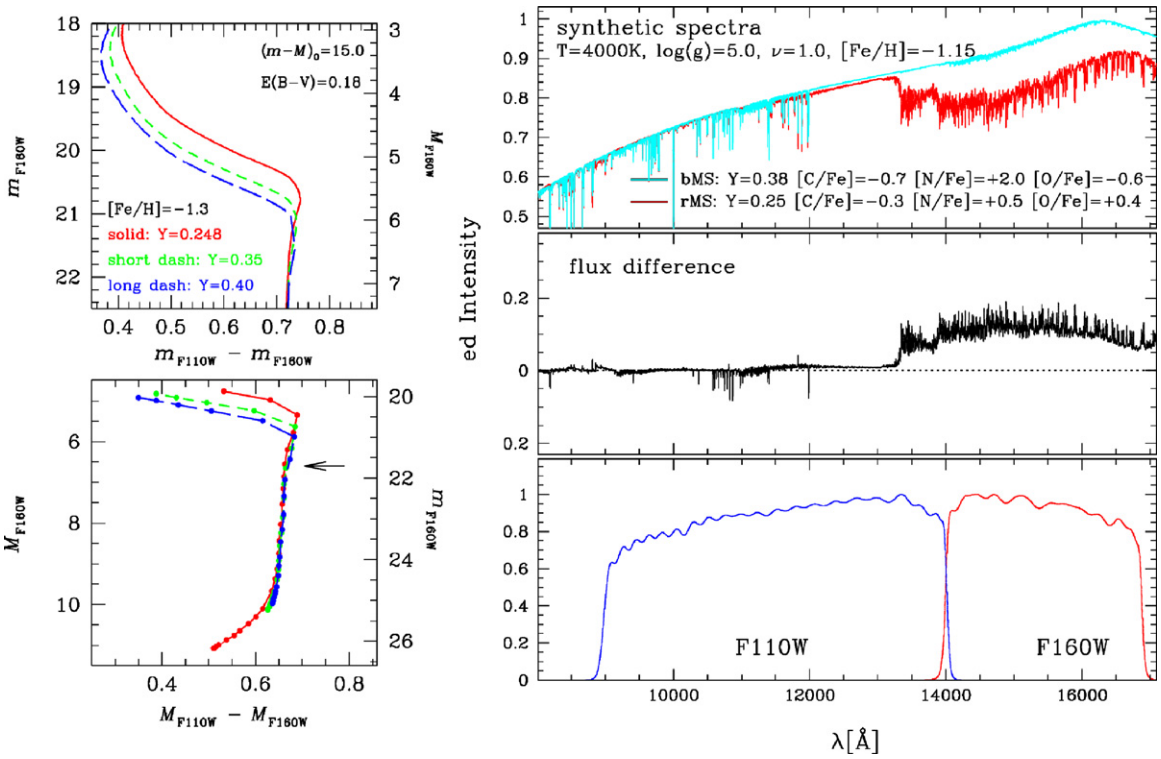

Figure 4. Left panels: theoretical isochrones for an age of 12 Gyr, a metallicity suitable for NGC 2808 and various assumptions about the initial He content (see labels). The upper left panel shows the theoretical absolute magnitudes and colors. In the lower left panel, we show—after applying a distance modulus $(m - M)_0 = 15.0$ and a reddening $E(B - V) = 0.18$, in order to make the comparison with the upper right panel of Figure 3 easier—the location in the CMD of the stellar models with mass in the range from 0.0894 $M_\odot$ to 0.65 $M_\odot$. The arrow marks the approximate location along the MS loci of the VLM stellar model with effective temperature and gravity values consistent with those adopted for computing the model atmospheres. Right panels: comparison of the synthetic spectra of a bMS star (cyan) and an rMS star (red, see the text for more details) difference between the synthetic spectrum of a bMS and an rMS star (middle). Normalized responses of the F110W and F160W WFC3/NIR *HST* filters (bottom).

(A color version of this figure is available in the online journal.)

Table 1
Average Chemical Abundances of bMS, mMS, and rMS Stars and Abundanced Adopted for the MS_I and the MS_{II}

MS	Y	[C/Fe]	[N/Fe]	[O/Fe]
rMS	0.25	−0.3	0.5	0.4
mMS	0.32	NA	NA	0.0
bMS	0.38	−0.7	2.0	−0.6
MS_I	0.25	−0.3	0.5	0.4
MS_{II}	0.38	−0.7	2.0	−0.6

For the MS_I and MS_{II}, we adopted a helium content of $Y = 0.25$ and $Y = 0.38$, respectively, as suggested by isochrone fitting on the upper MS (M12). For the MS_I, we assumed an average chemical abundance of O-rich stars ([O/Fe] = 0.4, as measured by Carretta et al. 2006) and adopted the carbon and nitrogen abundance ([C/Fe] = −0.3, [N/Fe] = 0.5) measured by Bragaglia et al. (2010). For the MS_{II}, we used [O/Fe] = −0.6 (the O abundance measured by Carretta et al. 2006 for the O-poor group), and [C/Fe] = −0.7, and [N/Fe] = 2.0 (as measured by Bragaglia et al. 2010 for a bMS star). Table 1 summarizes the adopted chemical abundances for the two sequences. For both MSs we used $T_{eff} = 4000$ K, $\log(g) = 5.0$, and a microturbolence 1.0 km s^{-1}. Our synthesis includes the following molecules in the Kurucz compilation: CO, C_2, CN, OH, MgH, SiH, H_2O, TiO (H_2O from Partridge & Schwenke 1997; TiO from Schwenke 1998), VO, and ZrO (B. Plez 2012, private communication) The resulting synthetic spectra (Figure 4, upper right panel) have been integrated over the transmission of the WFC3/IR F110W and the F160W filters (lower right panel) to produce synthetic magnitudes and colors. We found a $\Delta(M_{F110W} - M_{F160W}) = 0.10$ color difference between the simulated MS_I and MS_{II} stars, consistent with the observed color difference (Figure 2) at $m_{F160W} = 21.5$: $\Delta(m_{F110W} - m_{F160W}) = 0.06 \pm 0.01$ mag. The middle right panel of Figure 4 shows the flux difference as a function of the wavelength between the two MS spectra. The H_2O molecules have the strongest effect on the synthetic spectra and cause the significant lower flux of the rMS in the filter F160W. We consider the agreement between the simulated and observed color differences satisfactory, accounting for the high sensitivity to light-element abundances of the stellar spectra at these wavelengths, and that the adopted C and N abundances are based on the measurement on just one bMS and one rMS star (Bragaglia et al. 2010).

5. SUMMARY

The photometry presented in this Letter for NGC 2808 reveals, for the first time, multiple sequences in the near-infrared CMD of a GC. The brightest part of the CMD ($m_{F160W} < 20.5$) is consistent with three populations with different He and light-element abundance, as already noticed in previous papers based on visual photometry. The three MSs merge together at the luminosity of the MS bend while at fainter magnitudes, a combination of stellar structure and atmospheric effects makes the distinction among the different stellar populations more intricate. Our CMD allows us to identify at least two MSs.

A redder, more populated MS_I, which includes ∼65% of the MS stars, and that we associate with the first stellar generation, which has primordial He, and O–C-rich/N-poor stars, and an MS_{II}, with ∼35% of stars, corresponding to a second generation stellar population that is enriched in He and N and depleted in C and O. The MS_I of Figure 1 is the faint counterpart of the rMS identified by P07, whereas the MS_{II} corresponds to the lower mass counterpart of the mMS and bMS of P07.

This Letter provides the first detection of multiple populations with different helium and light-element abundances among VLM stars and extends the investigation by S11 to the near-IR. The fact that the signatures of abundance anti-correlation are also observed among fully convective M-dwarfs demonstrates, once and for all, that they have primordial origin and hence correspond to different stellar generations.

We are grateful to the referee for a thoughtful, thorough report that improved the accuracy and focus of the Letter. We warmly thank B. Plez for kindly providing molecular line lists. Support for this work has been provided by the IAC (grant 310394) and the Education and Science Ministry of Spain (grants AYA2007-3E3506 and AYA2010-16717). S.C. and G.P. thanks for financial support from PRIN INAF "Formation and early evolution of massive star clusters." G.P. acknowledges support by ASI under grants ASI-INAF I/016/07/0 and I/009/10/0.

REFERENCES

Allard, F., Homeier, D., & Freytag, B. 2011, in ASP Conf. Ser. 448, 16th Cambridge Workshop on Cool Stars, Stellar Systems, and the Sun, ed. C. M. Johns-Krull, M. K. Browning, & A. A. West (San Francisco, CA: ASP), 91
Allard, F., Homeier, D., & Freytag, B. 2012, Phil. Trans. R. Soc. A, 370, 2765
Anderson, A. J. 1997, PhD thesis, Univ. California, Berkeley
Anderson, J., & King, I. R. 2006, Instrument Science Report ACS 2006-01, 34 pp, 1
Anderson, J., Piotto, G., King, I. R., Bedin, L. R., & Guhathakurta, P. 2009, ApJ, 697, L58
Baraffe, I., Chabrier, G., Allard, F., & Hauschildt, P. H. 1997, A&A, 327, 1054
Bedin, L. R., Cassisi, S., Castelli, F., et al. 2005, MNRAS, 357, 1038
Bedin, L. R., Piotto, G., Anderson, J., et al. 2004, ApJ, 605, L125
Bedin, L. R., Piotto, G., Zoccali, M., et al. 2000, A&A, 363, 159
Bono, G., Stetson, P. B., VandenBerg, D. A., et al. 2010, ApJ, 708, L74
Bragaglia, A., Carretta, E., Gratton, R. G., et al. 2010, ApJ, 720, L41
Calamida, A., Bono, G., Stetson, P. B., et al. 2009, in IAU Symp. 258, The Ages of Stars (Cambridge: Cambridge Univ. Press), 189
Carretta, E., Bragaglia, A., Gratton, R. G., et al. 2006, A&A, 450, 523
Cassisi, S. 2012, Memorie della Societa Astronomica Italiana, ed. G. Bono & M. Zoccali (arXiv:1111.6464)
Cassisi, S., Castellani, V., Ciarcelluti, P., Piotto, G., & Zoccali, M. 2000, MNRAS, 315, 679
D'Antona, F., Bellazzini, M., Caloi, V., et al. 2005, ApJ, 631, 868
D'Antona, F., & Caloi, V. 2008, MNRAS, 390, 693
Gratton, R. G., Lucatello, S., Carretta, E., et al. 2011, A&A, 534, A123
Kurucz, R. L. 2005, Mem. Soc. Astron. Ital. Suppl., 8, 14
Lee, J.-W., Kang, Y.-W., Lee, J., & Lee, Y.-W. 2009, Nature, 462, 480
Marino, A. F., Villanova, S., Milone, A. P., et al. 2011, ApJ, 730, L16
Marino, A. F., Villanova, S., Piotto, G., et al. 2008, A&A, 490, 625
Milone, A. P., Bedin, L. R., Piotto, G., & Anderson, J. 2009, A&A, 497, 755
Milone, A. P., Bedin, L. R., Piotto, G., et al. 2008, ApJ, 673, 241
Milone, A. P., Piotto, G., Bedin, L. R., et al. 2012a, ApJ, 744, 58 (M12)
Milone, A. P., Piotto, G., Bedin, L. R., et al. 2012b, A&A, 540, A16
Partridge, H., & Schwenke, D. W. 1997, J. Chem. Phys., 106, 4618
Pietrinferni, A., Cassisi, S., Salaris, M., & Castelli, F. 2006, ApJ, 642, 797
Piotto, G., Bedin, L. R., Anderson, J., et al. 2007, ApJ, 661, L53 (P07)
Piotto, G., Milone, A. P., Bedin, L. R., et al. 2012, ApJ, submitted
Piotto, G., Villanova, S., Bedin, L. R., et al. 2005, ApJ, 621, 777
Sbordone, L., Bonifacio, P., & Castelli, F. 2007, in IAU Symp. 239, Convection in Astrophysics, ed. F. Kupka, I. Roxburgh, & K. Chan (Cambridge: Cambridge Univ. Press), 71
Sbordone, L., Salaris, M., Weiss, A., & Cassisi, S. 2011, A&A, 534, A9 (S11)
Schwenke, D. W. 1998, Faraday Discuss., 109, 321
Sosin, C., Dorman, B., Djorgovski, S. G., et al. 1997, ApJ, 480, L35
Yong, D., Grundahl, F., Johnson, J. A., & Asplund, M. 2008, ApJ, 684, 1159
Zoccali, M., Cassisi, S., Frogel, J. A., et al. 2000, ApJ, 530, 418